Electronic Supplementary Material (ESI) for Physical Chemistry Chemical Physics.

Supporting Information

Highly efficient utilization of light and charge separation over hematite photoanode achieved through noncontact photonic crystal film for photoelectrochemical water splitting

Wen-Yuan Yu,[d#] De-Kun Ma,*[ad] Dong-Peng Yang,*[b#] Xiao-Gang Yang,*[c] Quan-Long Xu,[d] Wei Chen [d] and Shaoming Huang *[b]

[a] *Zhejiang Key Laboratory of Alternative Technologies for Fine Chemicals Process, Shaoxing University, Shaoxing 312000, China*

[b] *School of Materials and Energy, Guangzhou Key Laboratory of Low-Dimensional Materials and Energy Storage Devices, Guangdong University of Technology, Guangzhou 510006, China*

[c] *Institute of Materials Science and Devices, Suzhou University of Science and Technology, Suzhou 215011, China*

[d] *Zhejiang Key Laboratory of Carbon Materials, Wenzhou University, Wenzhou 325027, China*

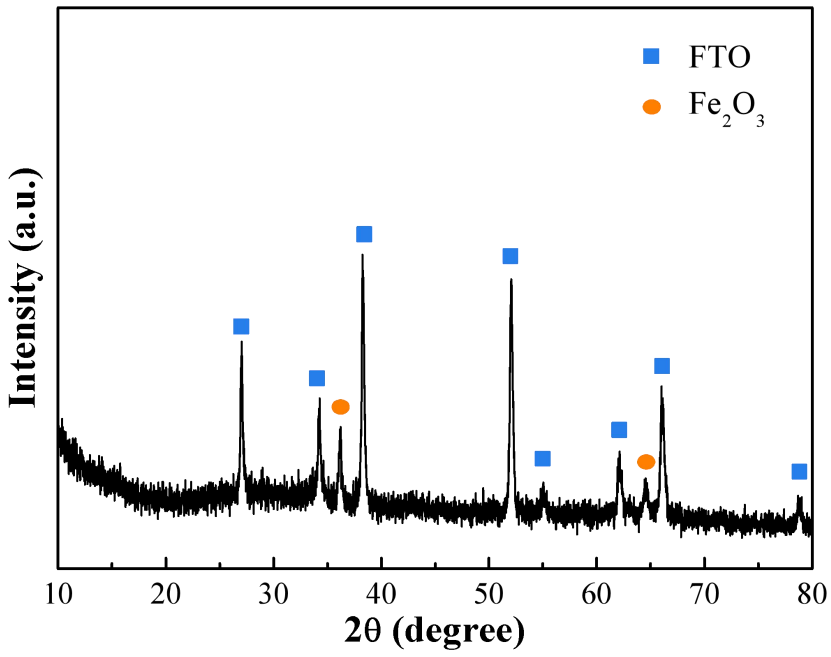

Fig. S1 XRD pattern of the as-prepared Fe_2O_3 nanorod array film grown on FTO glass.

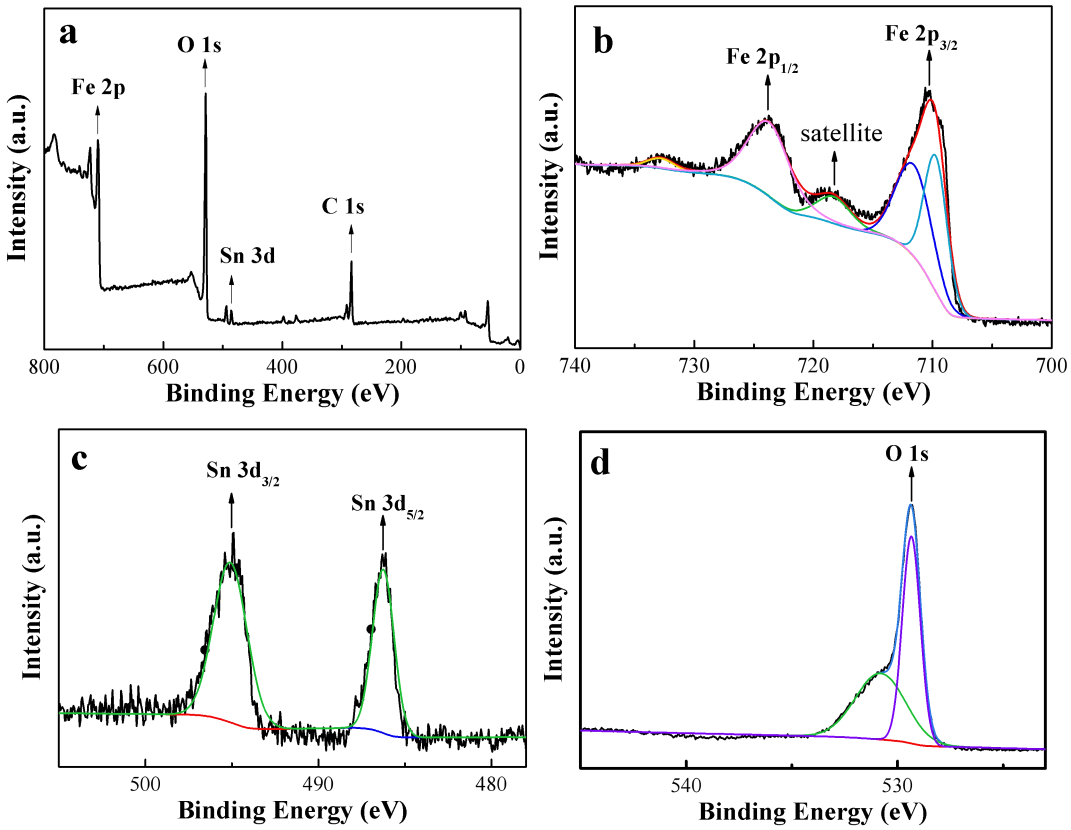

Fig. S2 XPS survey spectrum of the as-obtained α-Fe_2O_3 nanorod array film and corresponding high-resolution XPS spectra of Fe 2p (b), Sn 3d (c), and O 1s (d).

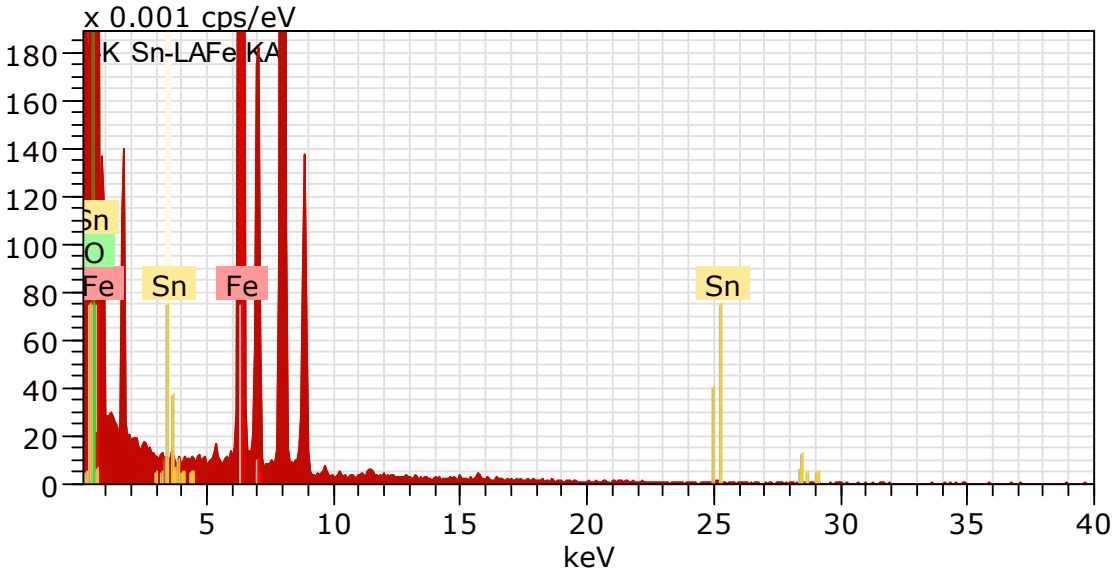

Fig. S3 EDX spectrum of the as-obtained α-Fe_2O_3 nanorod array

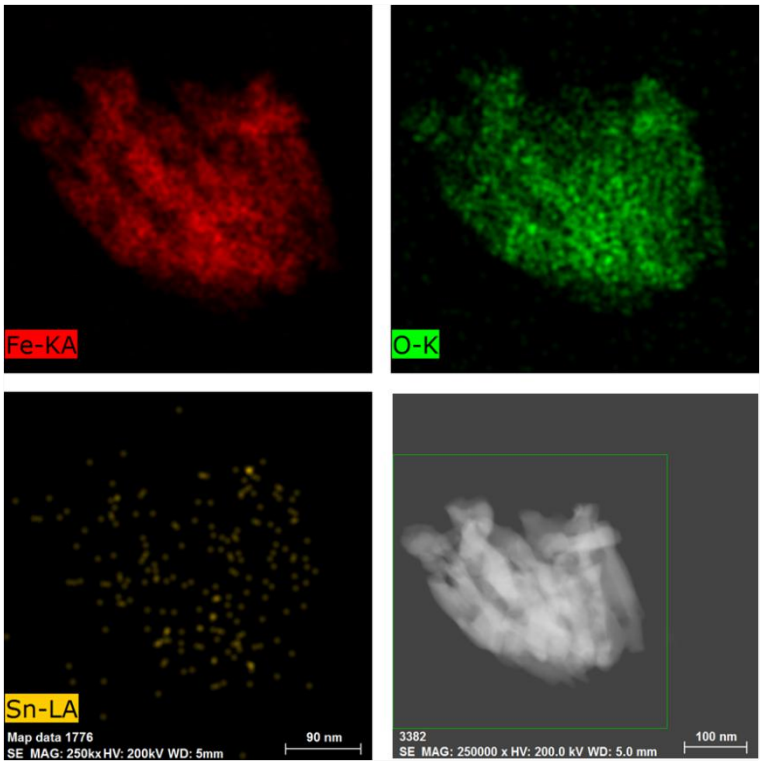

Fig. S4 Elemental mapping of the as-obtained α-Fe_2O_3 nanorod array and corresponding scanning transmission electron microscopy image.

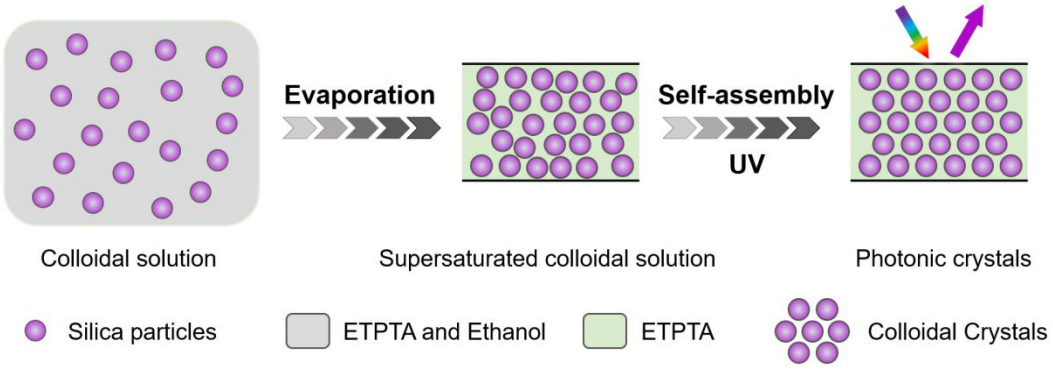

Fig. S5 Scheme for the fabrication of polymeric photonic crystal film.

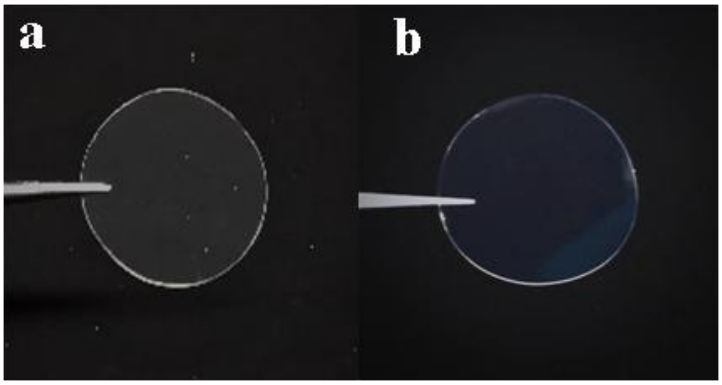

Fig. S6 Digital photos of the as-prepared ETPTA resin film (a) and PC film (b).

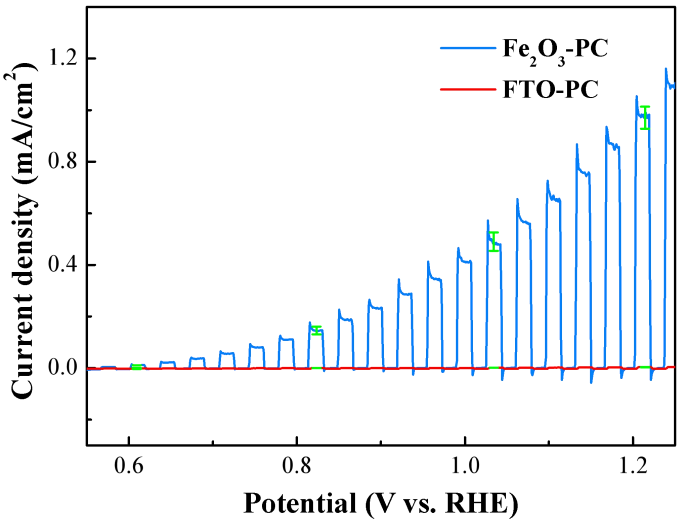

Fig. S7 Photocurrent-potential curves of Fe_2O_3-PC and FTO-PC under chopped light (AM 1.5, 100 mW/cm^2).

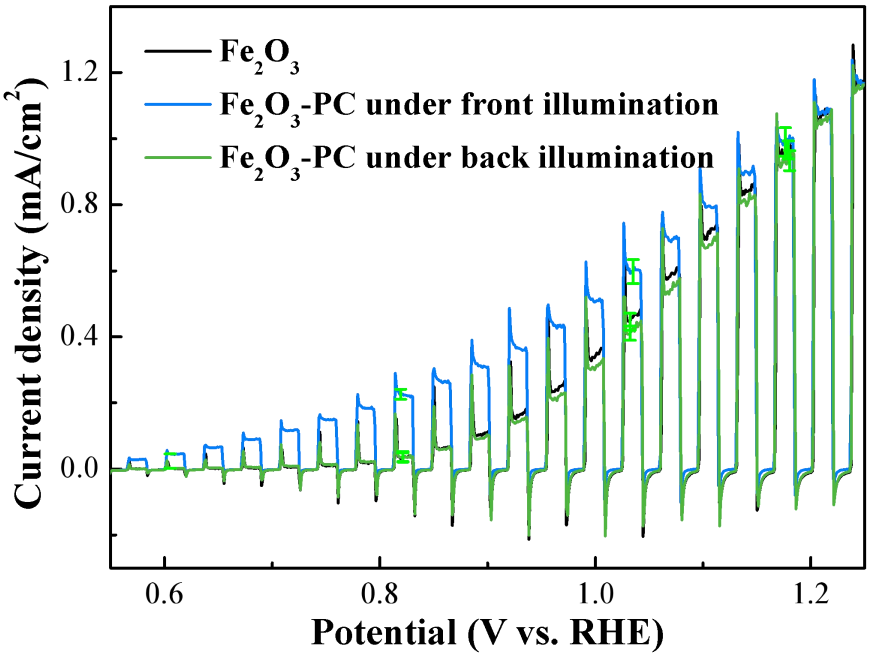

Fig. S8 Photocurrent-potential curves of Fe_2O_3-PC film under different illumination modes.

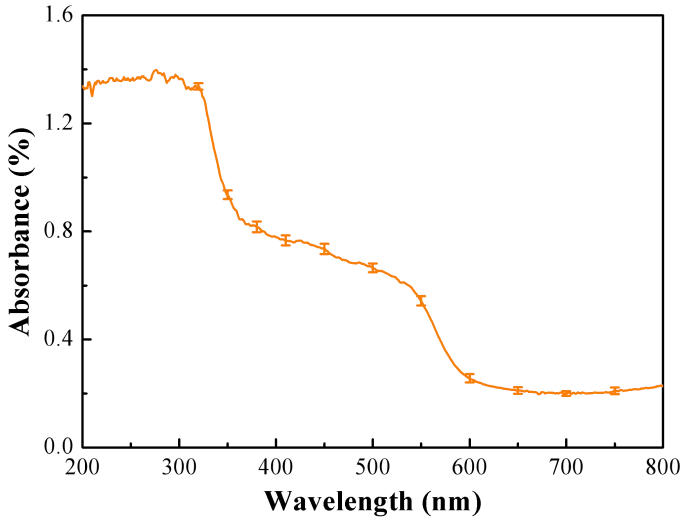

Fig. S9 UV-visible absorption spectrum of α-Fe_2O_3 nanorod array film.

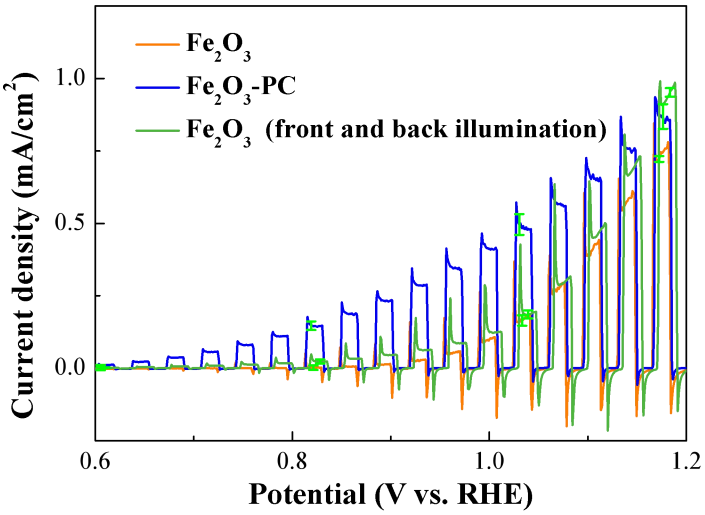

Fig. S10 Photocurrent-potential curves of α-Fe_2O_3 and α-Fe_2O_3-PC films under front illumination. (AM 1.5, 100 mW/cm^2) and Fe_2O_3 film under simultaneous front (AM 1.5, 100 mW/cm^2)- and back (AM 1.5, 60 mW/cm^2)-illumination, respectively.

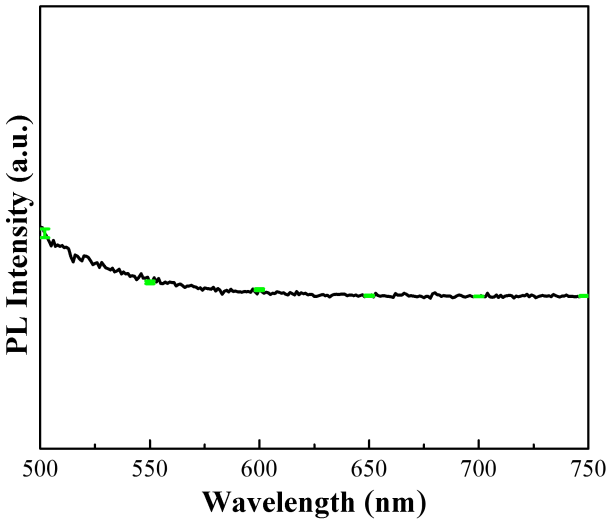

Fig. S11 PL spectrum of PC film under excitation wavelength of 400 nm at room temperature.

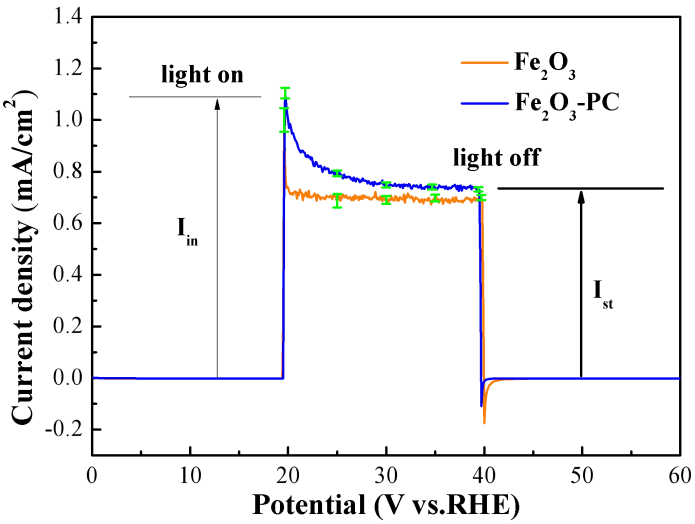

Fig. S12 Photocurrent-time curves of α-Fe_2O_3 and α-Fe_2O_3-PC films at an applied potential of 1.2 V vs. RHE. Taking the photocurrent current-time curve of α-Fe_2O_3-PC as an example, I_{in} and I_{st} were labeled.

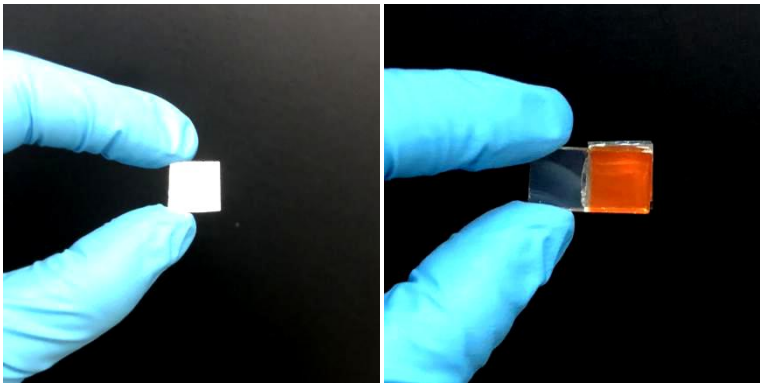

Fig. S13 Digital photos of HRM used in this work and the as-fabricated α-Fe_2O_3-HRM photoelectrode.

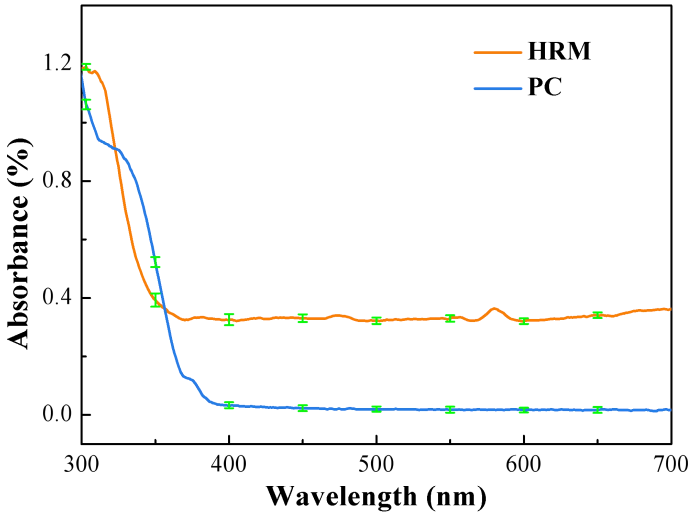

Fig. S14 UV-Vis absorption spectra of PC films and HRM.

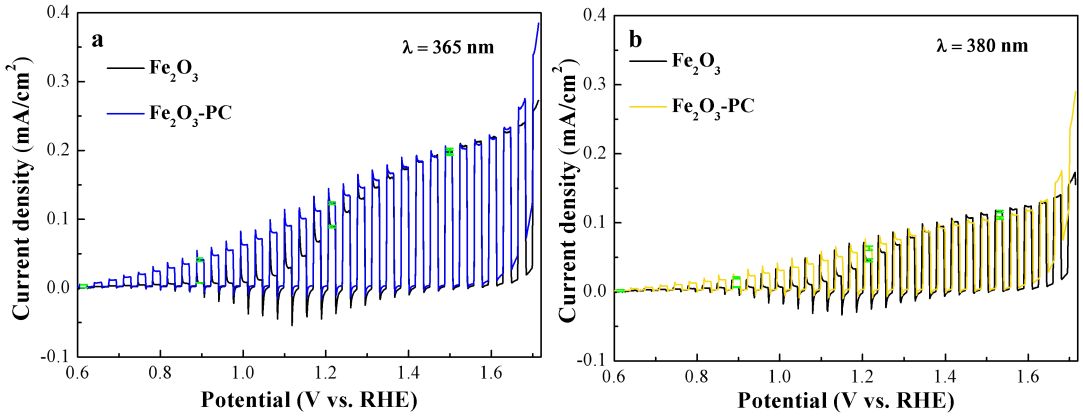

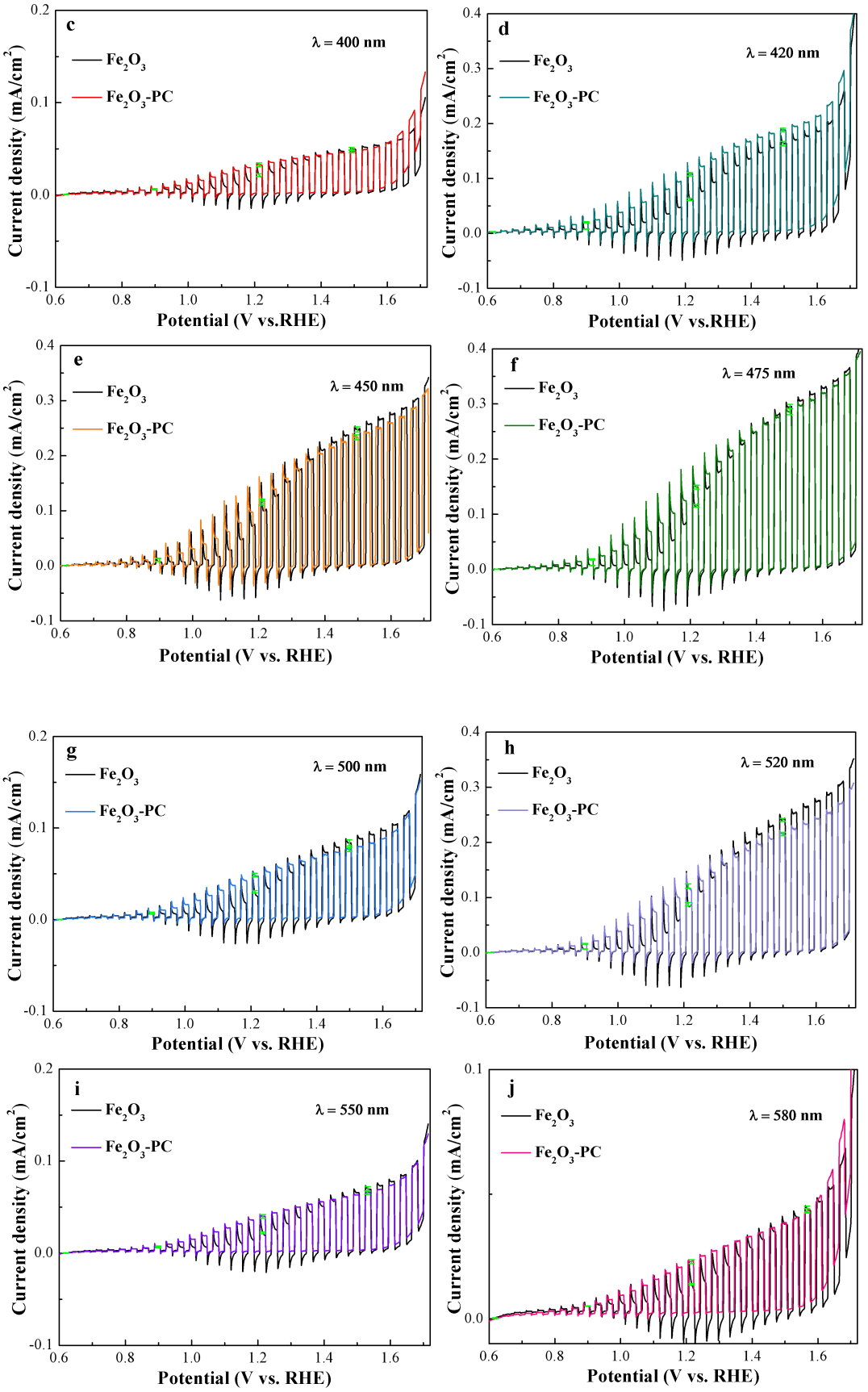
c
λ = 400 nm
Fe2O3
Fe2O3-PC
Current density (mA/cm2)
Potential (V vs.RHE)
d
λ = 420 nm
Fe2O3
Fe2O3-PC
Current density (mA/cm2)
Potential (V vs.RHE)
e
λ = 450 nm
Fe2O3
Fe2O3-PC
Current density (mA/cm2)
Potential (V vs. RHE)
f
λ = 475 nm
Fe2O3
Fe2O3-PC
Current density (mA/cm2)
Potential (V vs. RHE)
g
λ = 500 nm
Fe2O3
Fe2O3-PC
Current density (mA/cm2)
Potential (V vs. RHE)
h
λ = 520 nm
Fe2O3
Fe2O3-PC
Current density (mA/cm2)
Potential (V vs. RHE)
i
λ = 550 nm
Fe2O3
Fe2O3-PC
Current density (mA/cm2)
Potential (V vs. RHE)
j
λ = 580 nm
Fe2O3
Fe2O3-PC
Current density (mA/cm2)
Potential (V vs. RHE)

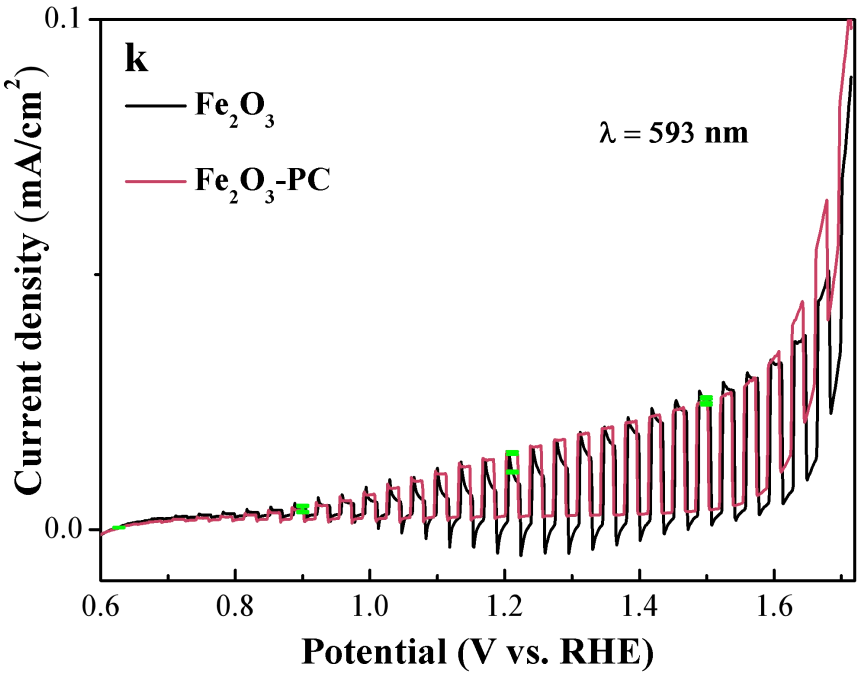

Fig. S15 Photocurrent versus potential curves of α-Fe_2O_3 and α-Fe_2O_3-PC under different monochromatic light irradiation. Here the monochromatic light was obtained through bandpass filters with a certain width. The wavelength values used here corresponds to center wavelength of the filter.

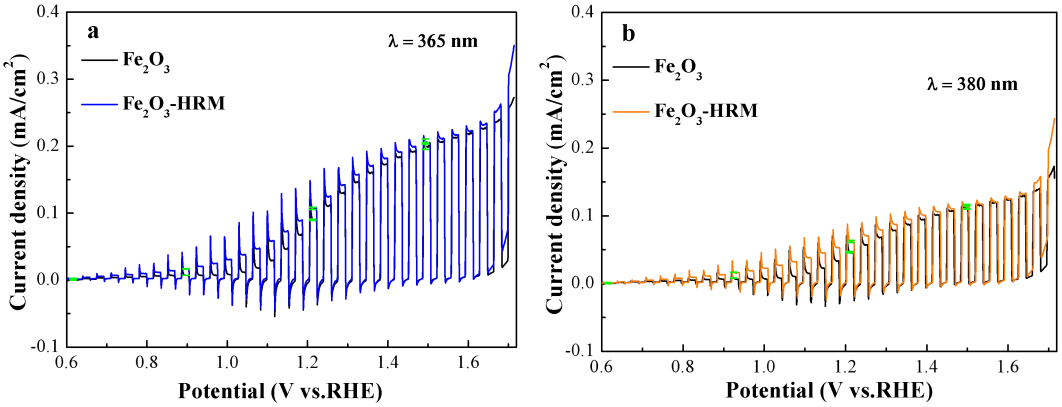

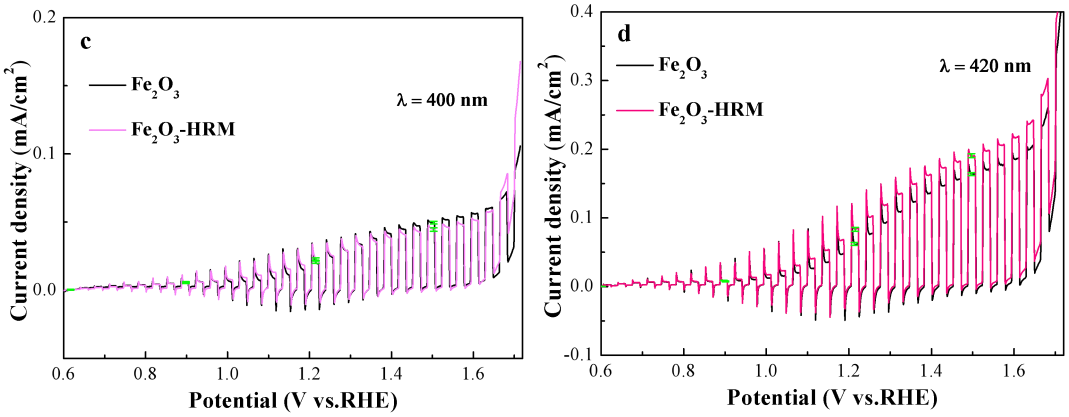
c
Fe2O3
Fe2O3-HRM
λ = 400 nm
Current density (mA/cm2)
Potential (V vs.RHE)

d
Fe2O3
Fe2O3-HRM
λ = 420 nm
Current density (mA/cm2)
Potential (V vs.RHE)

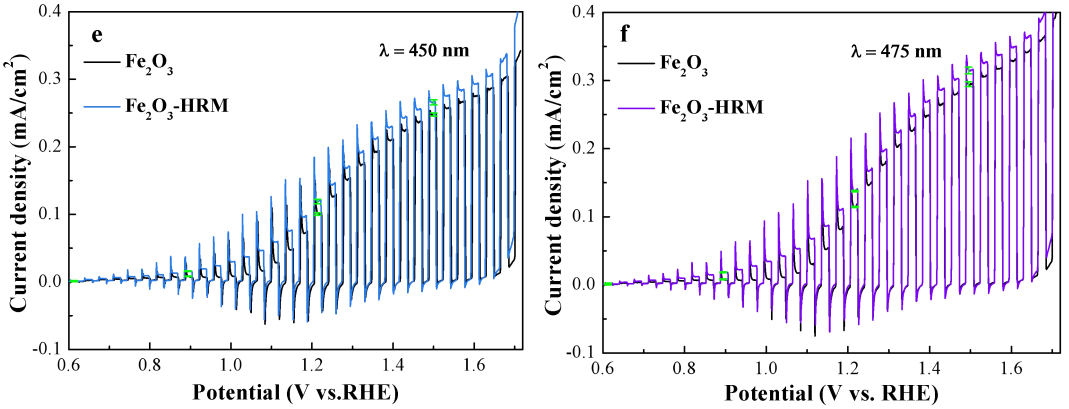
e
Fe2O3
Fe2O3-HRM
λ = 450 nm
Current density (mA/cm2)
Potential (V vs.RHE)

f
Fe2O3
Fe2O3-HRM
λ = 475 nm
Current density (mA/cm2)
Potential (V vs. RHE)

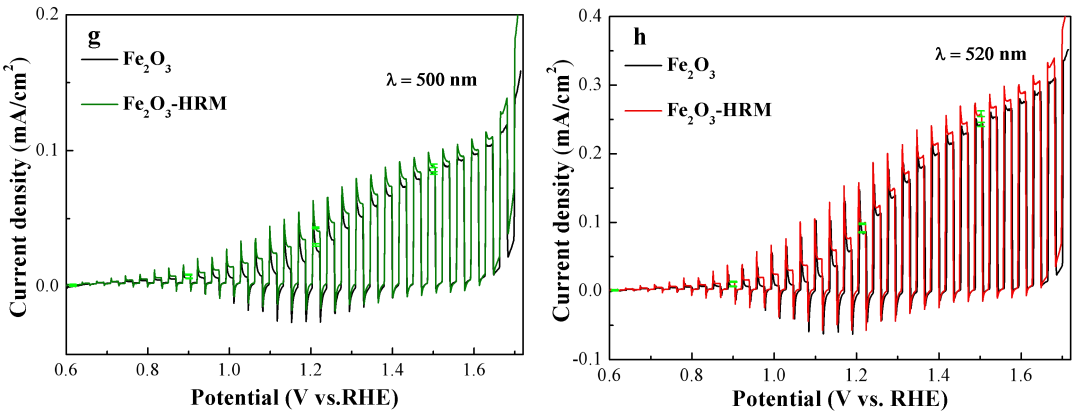
g
Fe2O3
Fe2O3-HRM
λ = 500 nm
Current density (mA/cm2)
Potential (V vs.RHE)

h
Fe2O3
Fe2O3-HRM
λ = 520 nm
Current density (mA/cm2)
Potential (V vs. RHE)

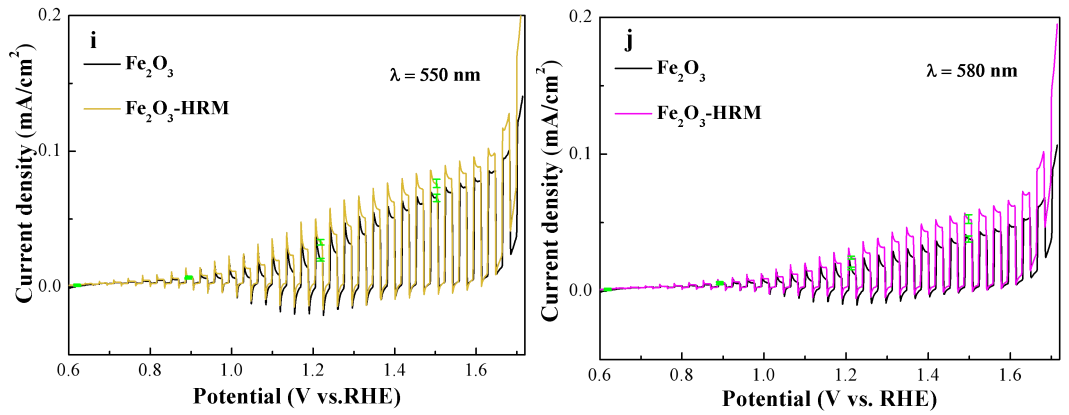
i
Fe2O3
Fe2O3-HRM
λ = 550 nm
Current density (mA/cm2)
Potential (V vs.RHE)

j
Fe2O3
Fe2O3-HRM
λ = 580 nm
Current density (mA/cm2)
Potential (V vs. RHE)

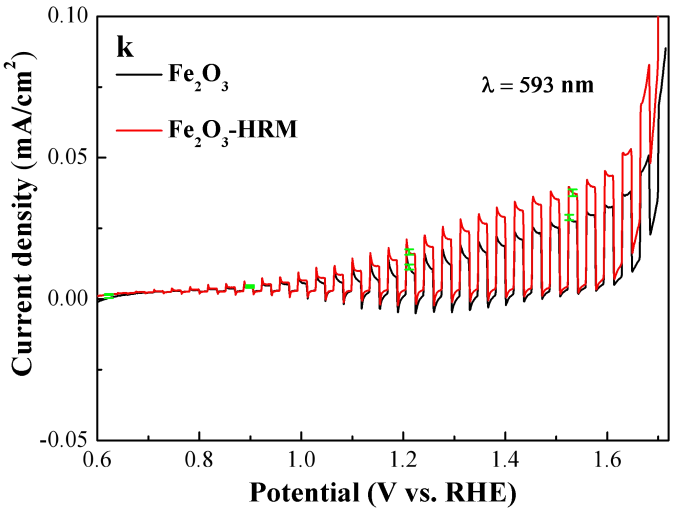

Fig. S16 Photocurrent versus potential curves of α-Fe_2O_3 and α-Fe_2O_3-HRM under different monochromatic light irradiation.

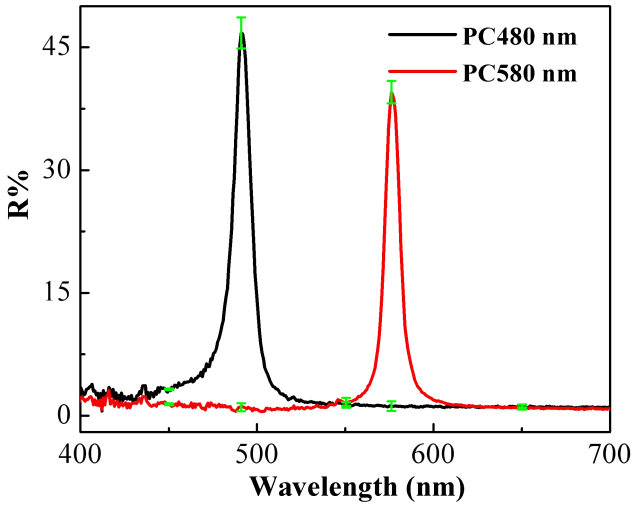

Fig. S17 Reflectance spectra obtained through silica particles with sizes of 170 nm (black line) and 195 nm (red line), respectively.

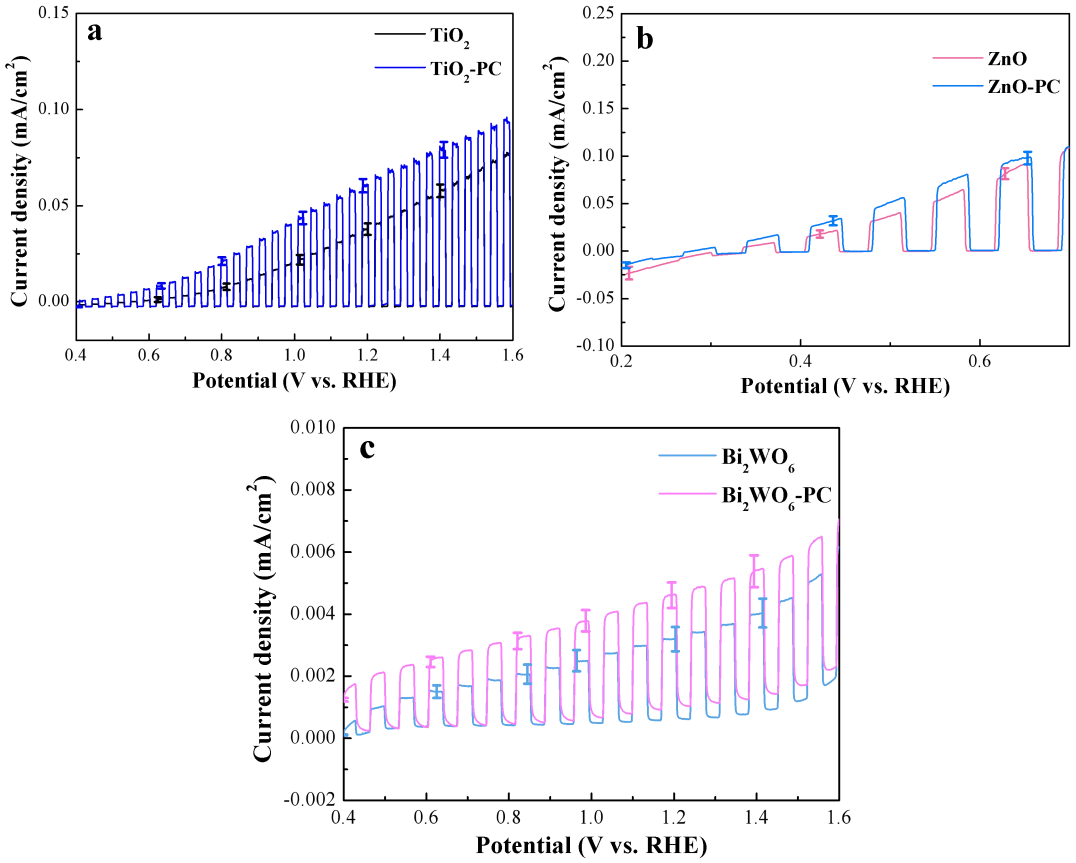

Fig. S18 Photocurrent-potential curves of TiO_2, ZnO, and Bi_2WO_6 photoanodes under chopped light (AM 1.5G, 1 mW/cm^2) in the absence of PC film and in the presence of PC film.

Table S1. Photoelectrochemical activities of some typical α-Fe_2O_3 nanostructures photoanodes and modified α-Fe_2O_3 photoanodes with different strategies.

Materials	Reaction conditions	V_{on} [V vs.RHE]	Photocurrent density at 1.0 V (vs.RHE) [mA/cm^2]	Reference
Fe_2O_3 on Au nanohole array	1M NaOH (pH 13.6)	0.8	0.2	[1]
TiO_2/Ti:Fe_2O_3 NRs	1M KOH (pH 13.6)	0.7	0.25	[2]
$NiFeO_X$:Fe_2O_3	1M NaOH (pH 13.6)	0.62	0.38	[3]
Sn:Fe_2O_3 NWs	1M KOH (pH 13.6)	0.6	0.59	[4]
FeOOH/Fe_2O_3	1M NaOH (pH 13.6)	0.8	0.45	[5]
$TiSi_2$/Fe_2O_3	1M NaOH (pH 13.6)	0.85	0.25	[6]
Fe_2O_3 containing oxygen vacancy	1M NaOH (pH 13.6)	0.75	0.58	[7]
Fe_2O_3 champion nanostructures	1M NaOH (pH 13.6)	0.75	0.16	[8]
(110) facets orientated Fe_2O_3	0.5 M H_2O_2 /1M NaOH (pH 13.6)	0.6	0.37	[9]
Fe_2O_3 of surface state removal	1M KOH (pH 13.6)	0.7	0.35	[10]
PC-Fe_2O_3	1M KOH (pH 13.6)	0.55	0.41	This work

References

1 J. T. Li, S. K. Cushing, P. Zheng, F. Meng, D. Chu and N. Q. Wu, *Nat. Commun.*, 2013, **4**, 2651.

2 Z. B. Luo, T. Wang, J. J. Zhang, C. C. Li, H. M. Li and J. L. Gong, *Angew. Chem. Int. Ed.*, 2017, **56**, 12878–12882.

3 C. Du, X. Yang, M. Mayer, T. H. Hoyt, J. Xie, G. McMahon, G. Bischoping and D. Wang, *Angew. Chem. Int. Ed.*, 2013, **52**, 12692–12695.

4 M. Li, Y. Yang, Y. Ling, W. Qiu, F. Wang, T. Liu, Y. Song, X. Liu, P. Fang, Y. Tong and Y. Li,

Nano Lett., 2017, **17**, 2490–2495.

5 Q. Yu, X. G. Meng, T. Wang, P. Li and J. H. Ye, *Adv. Funct. Mater.*, 2015, **25**, 2686–2692.

6 Y. J. Lin, S. Zhou, S. W. Sheehan and D. Wang, *J. Am. Chem. Soc*., 2011, **133**, 2398–2401.

7 Z. L. Wang, X. Mao, P. Chen, M. Xiao, S. A. Monny, S. C. Wang, M. Konarova, A. J. Du and L. Z. Wang, *Angew. Chem. Int. Ed.*, 2019, **58**, 1030−1034.

8 S. C. Warren, K. Voitchovsky, H. Dotan, C. M. Leroy, M. Cornuz, F. Stellacci, C. Hebert, A. Rothschild and M. Grätzel, *Nat. Mater*., 2013, **12**, 842–849.

9 S. Kment, P. Schmuki, Z. Hubicka, L. Machala, R. Kirchgeorg, N. Liu, L. Wang, K. Lee, J. Olejnicek, M. Cada, I. Gregora and R. Zboril, *ACS Nano*, 2015, **9**, 7113–7123.

10 O. Zandi and T. W. Hamann, *J. Phys. Chem. Lett*., 2014, **5**, 1522–1526.